BIOCHEMISTRY
including biophysical chemistry & molecular biology
Article

Biochemistry **2009,** *48,* 7457–7464 7457
DOI: 10.1021/bi900851q

Mapping of the Allosteric Network in the Regulation of α-Isopropylmalate Synthase from *Mycobacterium tuberculosis* by the Feedback Inhibitor L-Leucine: Solution-Phase H/D Exchange Monitored by FT-ICR Mass Spectrometry†

Patrick A. Frantom,[‡,§,△] Hui-Min Zhang,[‡,∥,⊥] Mark R. Emmett,[∥,#] Alan G. Marshall,[∥,#] and John S. Blanchard*[,§]

[§]*Department of Biochemistry, Albert Einstein College of Medicine, 1300 Morris Park Avenue, Bronx, New York 10461,* [∥]*Ion Cyclotron Resonance Program, National High Magnetic Field Laboratory, Florida State University, 1800 East Paul Dirac Drive, Tallahassee, Florida 32310-4005,* [⊥]*Institute of Molecular Biophysics, Florida State University, Tallahassee, Florida 32306, and* [#]*Department of Chemistry and Biochemistry, Florida State University, Tallahassee, Florida 32306* [‡]*P.A.F. and H.-M.Z. contributed equally to this work* [△]*Present address: Department of Chemistry, University of Alabama, 250 Hackberry Lane, Tuscaloosa, AL 35487*

Received May 19, 2009; Revised Manuscript Received June 29, 2009

ABSTRACT: As it is becoming accepted that allosteric regulation can occur through a change in local conformational equilibria as opposed to a change in overall static structure, a thorough description of the structural aspects of these types of mechanisms will be essential to understanding this fundamental biological process. Here we report the experimental identification of key regions of conformational perturbation in the allosteric network of a large (144 kDa), multidomain enzyme by use of solution-phase hydrogen/deuterium exchange. Large perturbations in the regulatory domain induced by effector molecule binding are linked to a very specific, targeted perturbation in the active site, some 50 Å away. Binding of L-leucine to an enzyme variant (Y410F) that is kinetically insensitive to effector binding was shown to elicit similar changes in the regulatory domain, but perturbs an alternate region of the catalytic domain, consistent with the proposed allosteric mechanism. These results comprise one of the first reports of an experimentally mapped allosteric mechanism in a protein of this size and provide necessary information to be used toward the development of allostery-based drugs or enzymes with engineered regulatory properties.

Understanding the mechanism of allosteric regulation in proteins, in which an effector molecule exerts influence at a distal site, has been a central pursuit of biochemistry for over 40 years (*1*). For some enzyme systems a detailed mechanism for allosteric regulation has been established based on structural changes to the protein (*2*, *3*). These mechanisms can be described as alterations in quaternary structure or stabilization of an open vs closed complex upon effector binding and are consistent with a two-state structural model of allosteric regulation. However, there are now numerous reports of systems for which there is evidence for allosteric regulation in the absence of changes in quaternary structure or selective stabilization of static open and closed forms, including TonB-dependent transporters and the catabolite activator protein (*4*−*8*). In these cases, the allosteric mechanism has been described by invoking changes in local conformational equilibria, or protein dynamics, transmitted through a type of contact network between the binding site of the effector molecule and the active site. Because the role of protein dynamics in catalysis has received a great deal of attention over the past 10 years (*9*), it is not surprising that altered dynamics may play a role in allosteric regulation as well (*10*).

A major problem in invoking altered conformational equilibria is that these changes are difficult to measure. Crystallography has been the most prominent source of identifying structural changes upon effector binding, but as a static ensemble of structures there is little information about dynamics. NMR-derived solution structures and amide exchange experiments offer a more dynamic picture and have been used to verify changes in local equilibria upon effector binding (*4*, *11*), but these studies are limited by the size of the protein and the amount required for each experiment. The use of computational approaches has emerged as a method for elucidating possible networks (*8*), but more experimental-based methods are required.

Solution-phase amide hydrogen/deuterium exchange (HDX)[1] and high-resolution Fourier transform ion cyclotron resonance mass spectrometry (FT-ICR MS) coupled to computer-aided data analysis offer a nonperturbing probe of conformational changes (reflected by the change in deuterium incorporation for the amide backbone hydrogens in each of a series of proteolytic peptide fragments) in proteins and their complexes (*12*). The method has been validated by the excellent agreement between HDX rates determined by FT-ICR MS and NMR on the same protein (*13*) and has revealed detailed conformational changes on formation of protein complexes in HIV-1 capsid protein assembly (*14*), a viral molecular motor (*15*), and in elucidating drug resistance mechanisms for antitumor drugs targeting KIT kinase (*16*). Here, we apply the method to the mapping of an

†This work was supported by NIH Grants AI33696 (J.S.B.) and GM78359, NSF Division of Materials Research through DMR-0654118, the State of Florida, and a fellowship from the Charles H. Revson Foundation (P.A.F.).

*Address correspondence to this author. Telephone: (718) 430-3096. Fax: (718) 430-8565. E-mail: blanchar@aecom.yu.edu.

[1]Abbreviations: HDX, hydrogen/deuterium exchange; FT-ICR MS, Fourier transform ion cyclotron resonance mass spectrometry; *Mt*IPMS, *Mycobacterium tuberculosis* isopropylmalate synthase; α-KIV, α-ketoisovalerate; DmpG/DmpF, bifunctional aldolase/dehydrogenase.

Published on Web 07/01/2009

allosteric pathway from the effector binding site to the catalytic site based on changes in local conformational equilibria in a large (144 kDa), multidomain protein.

The enzyme α-isopropylmalate synthase (IPMS) catalyzes the first step in the biosynthesis of L-leucine. As such, it is subject to feedback regulation by L-leucine (*17*). In *Mycobacterium tuberculosis*, the biosynthetic pathway for L-leucine has been shown to be essential for growth *in vivo*, suggesting that enzymes in this pathway are possible targets for the design of new antitubercular therapeutics (*18*). L-Leucine acts as a V-type allosteric inhibitor and displays slow-onset kinetics (*19*). The three-dimensional structure of the *M. tuberculosis* IPMS (*Mt*IPMS) shows that the enzyme is a homodimer (72 kDa monomer) consisting of three domains (Figure 1A): an N-terminal TIM-barrel catalytic domain (residues 51−368), a subdivided linker domain (subdomain I includes residues 369−424, and subdomain II includes residues 434−490), and a C-terminal regulatory domain (residues 491−644) (*20*). When crystallized in the presence of L-leucine, one molecule of inhibitor/monomer is bound at the dimer interface of the regulatory domains, over 50 Å from the active site. When the crystallographically determined structures in the presence and absence of L-leucine are compared, there is closure of a small loop (residues 560−565) over the L-leucine binding site, but no conclusive structural changes are observed at the active site. Additional experiments demonstrate that the binding of L-leucine does not affect the quaternary structure of the enzyme (*21*). Taken together, these results suggest a mechanism of allosteric regulation involving interdomain communication via a change in conformational equilibria rather than changes in a static structure.

Recently, we have reported that substitutions of conserved residues at the interface of the linker and catalytic domains (40 Å from the L-leucine binding site) resulted in catalytically competent enzyme variants with altered inhibition kinetics (*22*). Two of the substitutions altered the enzyme's affinity for L-leucine despite their distance from the regulatory domain. However, the most drastic effect was the ablation of inhibition caused by L-leucine binding due to the substitution of a strictly conserved tyrosine residue (Y410) with phenylalanine (Figure 1B). These results are consistent with an allosteric network linking the regulatory and active sites, which can be disrupted by the Y410F substitution.

As drug design expands from active site-based therapeutics to include small molecules that will affect the dynamics of a protein to achieve either inhibition or activation, it will be critical to have a detailed understanding of the architecture of such allosteric networks (*23*). Here we report the experimental mapping of important regions in the allosteric network of *Mt*IPMS inhibition by L-leucine. The involvement of these regions in the allosteric signal was confirmed by use of the L-leucine-resistant Y410F *Mt*IPMS enzyme.

MATERIALS AND METHODS

Materials. Protease type XIII from *Aspergillus saitoi* was purchased from Sigma Aldrich. Protease type XIII provides sequence coverage superior to that for previously conventional pepsin (*24*). Potassium phosphate (monobasic and dibasic) and magnesium chloride were purchased from Fisher Biotech (Fair Lawn, NJ). HPLC grade H_2O and acetonitrile were purchased from VWR International (Suwanee, GA). Deuterium oxide and formic acid were purchased from Sigma Aldrich.

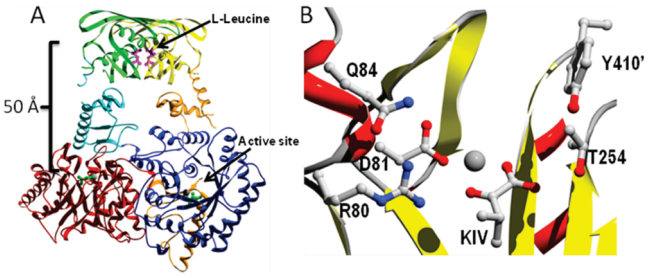

FIGURE 1: Ribbon drawing of the three-dimensional structure of α-isopropylmalate synthase from *M. tuberculosis*. (A) Domains colored red and blue, orange and cyan, and yellow and green correspond to the catalytic, linking, and regulatory domains, respectively, of each monomer. L-Leucine is colored purple in the regulatory domain. The substrate (α-KIV) is colored green to denote the active site. (B) Detailed rendering of the active site featuring the divalent metal, ketoisovalerate substrate, and the Y410′ residue.

Protein Preparation. Wild-type and Y410F *Mt*IPMS were both purified as previously described(*22*). Briefly, cells were lysed by sonication in the presence of Complete protease inhibitors (Roche), lysozyme, and DNase I in 20 mM TEA, pH 7.8, containing 300 mM NaCl and 50 mM imidazole, and the soluble extract was recovered after two centrifugations at 47000 × g. The clear soluble fraction was loaded onto a nickel-NTA column (100 mL) and eluted with a linear 50−500 mM imidazole gradient in 20 mM TEA, pH 7.8, containing 300 mM NaCl. The peak fractions were pooled and dialyzed against 10 L of 20 mM TEA, pH 7.8. The dialysate was loaded onto a Mono-Q column and eluted with a linear 0−500 mM NaCl gradient in 20 mM TEA, pH 7.8. The peak fractions were pooled and dialyzed against 10 L of 20 mM TEA, pH 7.8. The dialysate was made 1 M in $(NH_4)_2SO_4$, loaded onto a phenyl-Sepharose column, and eluted with a linear 1−0 M $(NH_4)_2SO_4$ gradient in 20 mM TEA, pH 7.8. Fractions containing pure *Mt*IPMS were pooled and concentrated. After concentration, the *Mt*IPMS solution was dialyzed against 10 L of 20 mM TEA, pH 7.8, containing 2 mM EDTA and after that dialyzed versus 10 L of 20 mM TEA, pH 7.8. The enzyme was stored at −20 °C in 50% glycerol. Directly prior to HDX experiments, the enzyme was dialyzed extensively against 20 mM potassium phosphate, pH 7.5, and 20 mM $MgCl_2$. After dialysis, the enzyme was concentrated to approximately 80 μM.

Hydrogen/Deuterium Exchange. The entire HDX experiment was automated with a LEAP robot (HTS PAL; Leap Technologies, Carrboro, NC). A 5 μL stock of *Mt*IPMS/Y410F *Mt*IPMS mutant (40 μM) was mixed with 45 μL of 20 mM potassium phosphate buffer, pH 7.5, and 20 mM $MgCl_2$ in D_2O to initiate each H/D exchange period. For L-leucine binding, the enzyme concentration was 20 μM, with 2500 μM L-leucine. L-Leucine was allowed to bind for 1 h prior to the start of the HDX experiments. For the blank control, the initial dilution was made in H_2O. For the zero-time control, quenching of the HDX and protease initiation were conducted simultaneously by addition of 50 μL of protease solution in 0.5% formic acid. The remaining HDX incubation periods were 0.5, 1, 2, 4, 8, 15, 30, 60, 120, 240, and 480 min, each followed by simultaneous quench and proteolysis. The controls and each of the incubation periods were performed in triplicate. H/D exchange was quenched by 1:1 (v/v) addition of protease solution (2-fold diluted saturated protease type XIII (*24*) solution) in 1.0% formic acid to decrease the final pH to ~2.3 and to start the 2 min protease digestion. The digested sample was then injected into a liquid chromatograph.

The entire HDX process was performed at ~0.4 °C controlled by a Huber power refrigerant (Peter Huber, Offenburg, Germany).

On-Line LC ESI FT-ICR MS/MS. A Jasco HPLC/SFC instrument (Jasco, Easton, MD) was interfaced to the LEAP robot to desalt and separate the *Mt*IPMS peptides after proteolysis. For LC, the protein digest was injected from a 10 μL loop to a Pro-Zap Prosphere HP C_{18} column (Grace Davidson, Deerfield, IL), HR 1.5 μm particle size, 500 Å pore size, 2.1 mm × 10 mm) (*25*). Peptides were eluted with a rapid gradient from 2% B to 95% B in 1.5 min (A, acetonitrile/H_2O/formic acid, 5/94.5/0.5; B, acetonitrile/H_2O/formic acid, 95/4.5/0.5) at a flow rate of 0.3 mL/min. A postcolumn splitter reduced the LC eluent flow rate to ~400−500 nL/min for efficient microelectrospray ionization (micro-ESI) (*26*).

The ionized LC eluent was directed to a custom-built hybrid LTQ 14.5 T FT-ICR mass spectrometer (ThermoFisher, San Jose, CA) (*27*). Mass spectra were collected from $400 < m/z < 2000$ at high mass resolving power ($m/\Delta m_{50\%} = 200000$ at m/z 400). The total data acquisition period for each sample was 6 min. External ion accumulation (*28*) was performed in the linear ion trap with a target ion population of 3 million charges collected for each FT-ICR measurement. LTQ-accumulated ions were transferred (~1 ms transfer period) through three octopole ion guides (2.2 MHz, 250 $V_{p\text{-}p}$) to a capacitively coupled (*29*) closed cylindrical ICR cell (55 mm i.d.) for analysis. The ion accumulation period was typically less than 100 ms during peptide elution, and the FT-ICR time-domain signal acquisition period was 767 ms (i.e., an overall duty cycle of ~1 s per acquisition). Automatic gain control (*30*) and high magnetic field (*31*) provided excellent external calibration mass accuracy (typically better than 500 ppb rms).

Nano-LC of the protease type XIII digested peptides was performed by use of a Nano-LC system (Eksigent, Dublin, CA). The LC system provided a true unsplit gradient at 300 nL/min from 15% B to 40% B in 40 min and 40% B to 98% B in 10 min (solvent A, 97.5% H_2O, 2% methanol, 0.5% formic acid; solvent B, 2% H_2O, 97.5% methanol, 0.5% formic acid). The *Mt*IPMS or Y410f *Mt*IPMS peptide fragments were separated over a 10 cm × 75 μm i.d. Pico-frit C18 column with a 15 μm i.d. tip. The column was packed with 5 μm particle size Proteoprep II packing (New Objective, Woburn, MA). The high voltage connection was made to the mobile phase through a stainless steel union that was used to connect the Pico-frit column to the nano-LC.

The nano-LC effluent was analyzed on-line by positive ion microelectrospray with a custom-built 14.5 T FT-ICR MS. Data-dependent MS/MS was performed in the linear ion trap (collisional dissociation) for the 10 most abundant ion species. The raw file data were analyzed by Multiplierz (BLAIS Proteomics center) to generate a list of all the peaks. Data were sent to Mascot (Matrix Science Ltd., London) with *Mt*IPMS and Y410F *Mt*IPMS sequences added to the database for peptide identification. The Mascot searching parameters were set at 2 ppm for parent ion and 0.8 Da for LTQ fragment ions.

Data Analysis. Data were collected with Xcalibur software (ThermoFisher) and analyzed by a custom analysis package permitting reliable identification and accurate assignment of the deuterium incorporation in each of the *Mt*IPMS fragments in the mass spectrum. A Python program was developed to automatically draw deuterium incorporation vs time profiles for identical fragments of two proteins to be compared. Time-course deuterium incorporation levels were determined by an MEM fitting method (*13*).

RESULTS

Effect of L-Leucine Binding on Wild-Type MtIPMS. In order to experimentally map sites of altered dynamics upon L-leucine binding, backbone−amide HDX experiments were carried out for wild-type *Mt*IPMS in the presence or absence of L-leucine as described in Materials and Methods. Identical peptides identified for both uncomplexed and complexed protein provided total sequence coverage of 85% in this experiment, with the sequence gaps randomly located throughout the protein (Supporting Information Figure S1). Upon addition of L-leucine to the wild-type enzyme, the deuterium incorporation decreased for a number of identified peptides. When those peptides are mapped onto the sequence, approximately 45% of the residues belonging to the regulatory domain (residues 490−644) show decreased deuterium incorporation upon L-leucine binding. When these changes are mapped onto the three-dimensional structure of the regulatory domain, many of the protected peptides are in direct contact with the bound L-leucine (residues 516−536, 522−540, 560−570, and 617−632) (Figure 2A and Supporting Information Figure S2).[2] However, a number of regulatory domain peptides are not in direct contact with the inhibitor but nonetheless exhibit reduced exchange upon L-leucine binding (residues 488−495, 504−516, and 507−519) (Supporting Information Figure S2). Residues 504−519 form an antiparallel β-sandwich with residues 522−540 (which are in contact with L-leucine) that makes up the exterior of the regulatory domain. Residues 488−495 are located at the C-terminus of a helix that forms a junction between the regulatory and linker domains.

In contrast to the regulatory domain, minor changes are seen in the linker and catalytic domains upon L-leucine binding. One small peptide (residues 453−457) in the linker subdomain II shows increased protection (Figure 2B). These residues are located on a short helix that makes contact with two regions in the regulatory domain that also show decreased deuterium incorporation (residues 488−495 and 617−632). In the catalytic domain, only a single peptide exhibits a change in deuterium incorporation (Figure 2C). Residues 78−87 display a small decrease in deuterium incorporation. Based on the three-dimensional structure, these residues make up a helix in the active site (Figure 1B). This peptide contains several strictly conserved residues that are proposed to be important for orienting the substrate α-KIV and binding the catalytically necessary divalent metal ion (*20*).

Effect of L-Leucine Binding on Y410F MtIPMS. We recently reported the kinetic characterization of the Y410F mutant form of *Mt*IPMS which is insensitive to inhibition by L-leucine (*22*). In order to determine if the kinetic results for the Y410F substituted enzyme were the result of an altered inhibitory signal, experiments identical to those performed on the wild-type enzyme were performed on Y410F *Mt*IPMS. When L-leucine is bound to Y410F *Mt*IPMS, large changes in amide backbone exchange, nearly identical to those seen in the wild-type enzyme, are observed in the regulatory domain. Peptides involved in binding L-leucine (residues 516−540, 545−552, and 608−632) show a decrease in deuterium incorporation, as do regions not

[2]Due to asymmetry in the dimeric crystal structure, a plausible model of all interdomain interactions in the dimeric protein is not possible. In addition, the domain-swapped nature of the dimer makes it impractical to visualize the monomer as a single polypeptide chain. Thus we have represented the HDX results on a "pseudomonomer" consisting of residues chain A (1−360) and chain B (361−644).

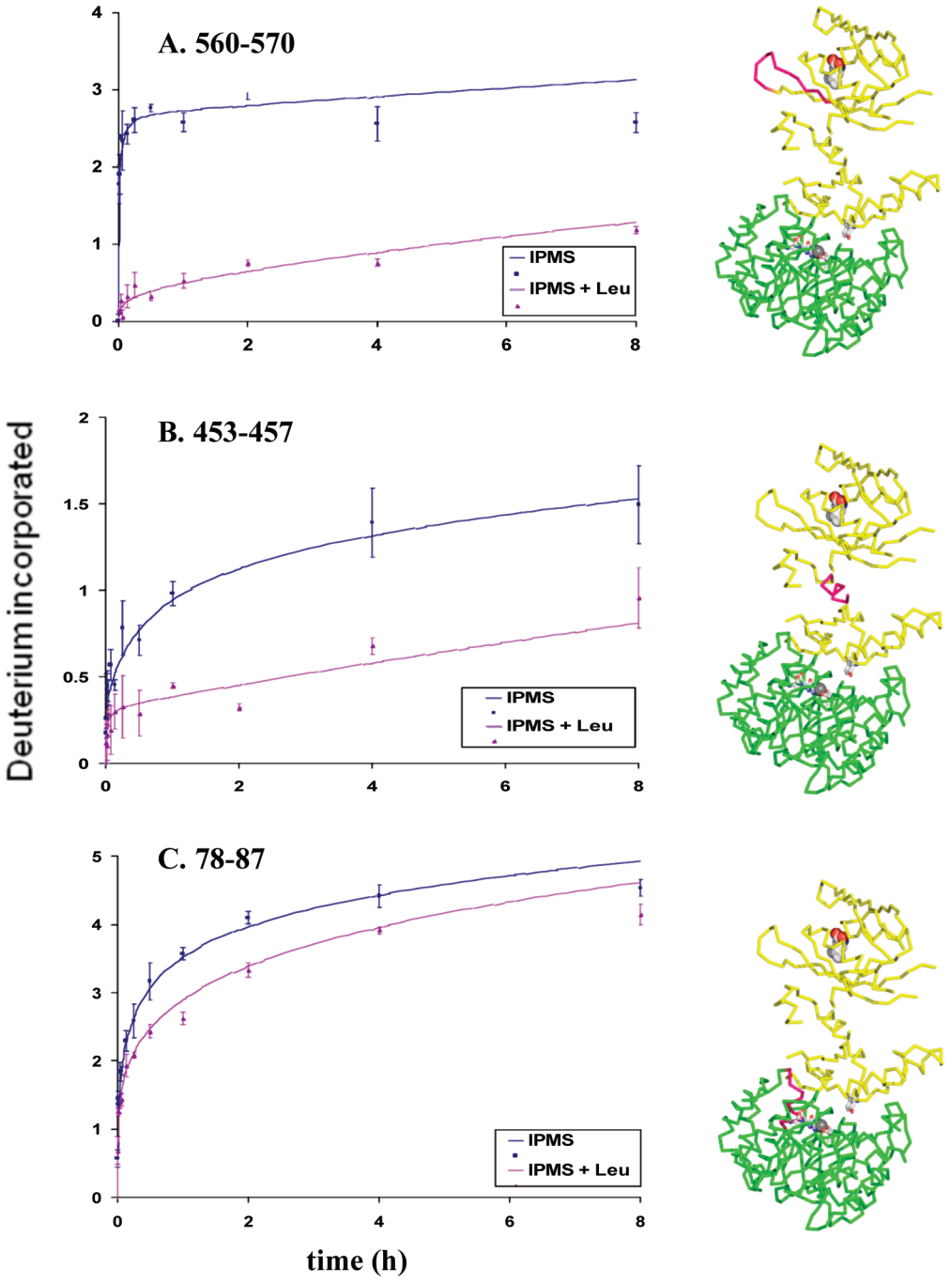

FIGURE 2: Deuterium incorporation curves for peptides in wild-type *Mt*IPMS in the absence and presence of L-leucine. Primary data are shown for residues 488−495 in the regulatory domain, residues 453−457 in the linker domain, and residues 78−87 in the catalytic domain. Three-dimensional structures are rendered as ribbons (chain A in green, chain B in yellow) with the corresponding peptide in pink.

directly involved in L-leucine binding (residues 488−499 and 500−515) (Figure 3A and Supporting Information Figure S3).

In the linker domain, only one fragment (residues 440−452) is protected upon L-leucine binding (Figure 3B). This peptide is adjacent to the peptide that displays decreased deuterium incorporation in the wild-type experiment (residues 453−457) and thus makes similar contacts with the regulatory domain (residues 608−632). In the catalytic domain, as for the wild-type enzyme, a single region exhibits decreased deuterium incorporation (residues 236−258) (Figure 3C). Residues 236−258 form a β-sheet located on the opposite side of the active site relative to the peptide identified in the wild-type enzyme. This region contains only one conserved residue (T254), proposed to interact with the substrate α-KIV (Figure 1B). The region of the active site identified in the wild-type experiment (residues 78−87) shows no changes in dynamics in the Y410F enzyme upon L-leucine binding.

Effects of the Y410F Substitution on the Apoenzyme. In order to determine what role the conserved Y410 residue plays in the dynamics of the enzyme, a comparison of the exchange kinetics from identical peptides was performed for wild-type and Y410F *Mt*IPMS in the absence of L-leucine. In this comparison, no regions within the regulatory domain display altered dynamics. A region in the subdomain II portion of the linker domain of the Y410F enzyme (residues 440−447 and 457−462) exhibited an increase in deuterium incorporation from exchange

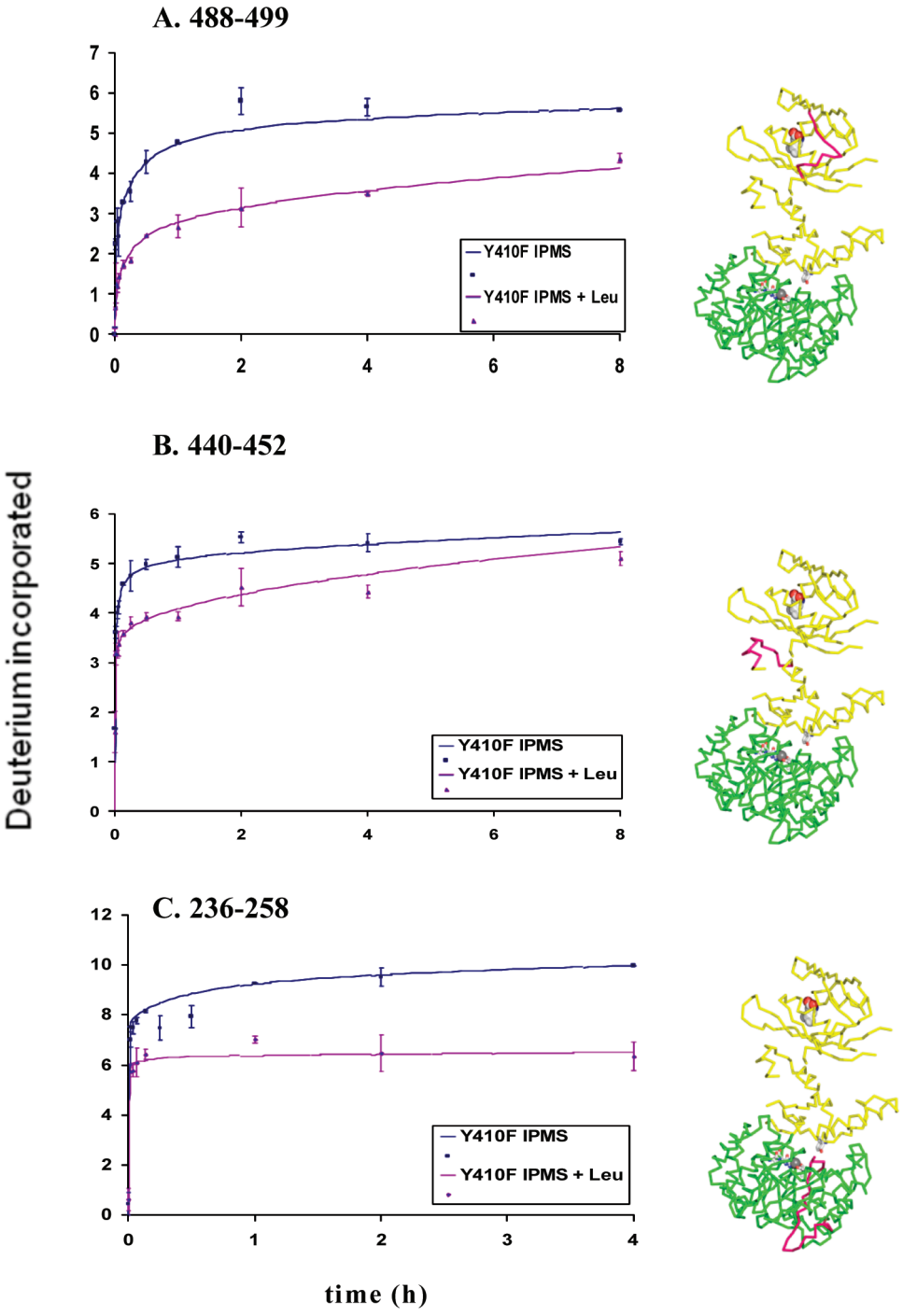

FIGURE 3: Deuterium incorporation time courses for peptides in Y410F *Mt*IPMS in the absence and presence of L-leucine. Primary data are shown for residues 488−499 in the regulatory domain, residues 440−452 in the linker domain, and residues 236−258 in the catalytic domain. Three-dimensional structures are rendered as ribbons (chain A in green, chain B in yellow) with the corresponding peptide in pink.

with solvent relative to the wild-type enzyme despite being over 16 Å away from the site of substitution. It is not surprising that numerous regions near the site of the substitution in subdomain I of the linker region are more exposed to solvent exchange in the Y410F enzyme relative to the wild type (peptides covering regions 362−370, 382−391, and 404−417). This accounts for a change in approximately 60% of the residues in this region, including the loop containing the Y410F substitution. Two regions in the catalytic domain displayed altered deuterium incorporation in the mutant enzyme. Residues 168−175 displayed increased deuterium incorporation in the mutant enzyme relative to the wild-type enzyme. This region is located directly adjacent to the site of substitution. Residues 78−87 were found to be more protected from solvent compared to the wild-type enzyme. As described above, residues 78−87 are located in the active site and correspond to the same region that is affected when the wild-type enzyme binds L-leucine.

DISCUSSION

As stated above, there are now many examples of allosteric mechanisms that operate in the absence of a change in shape of the protein. Instead, the binding of the allosteric effector molecule shifts the conformational equilibria of various regions of the protein to affect either catalysis or the affinity for a ligand. Based

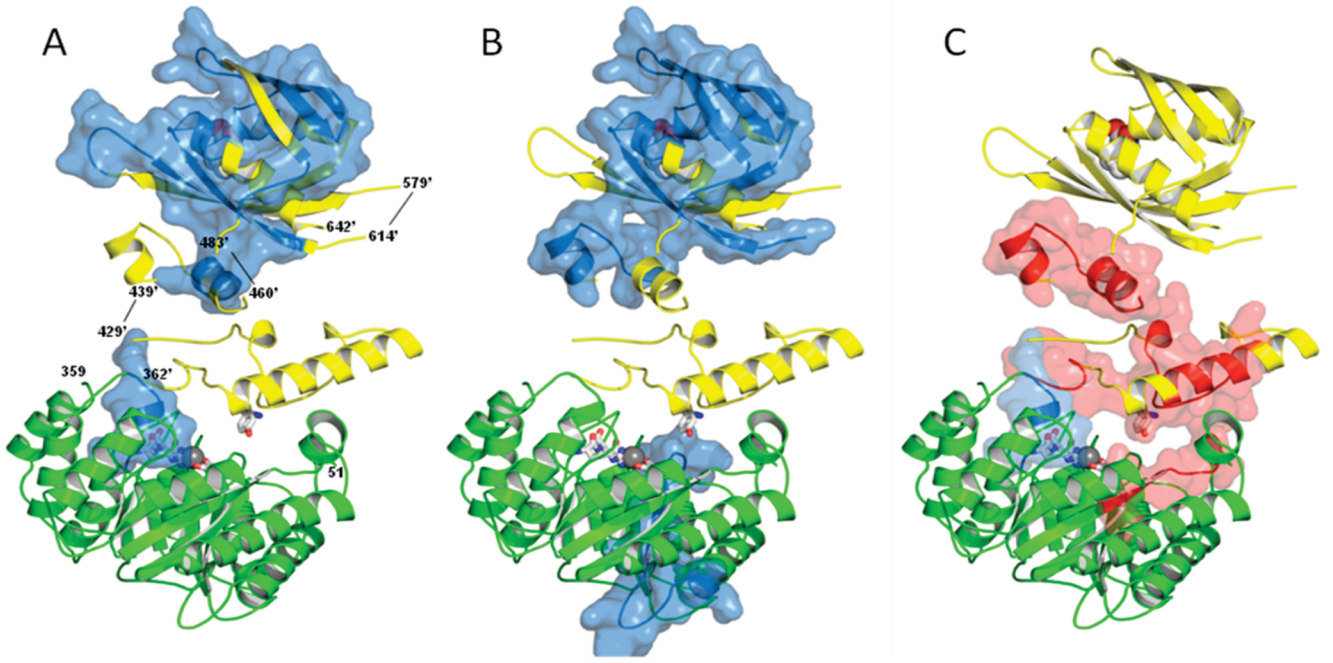

FIGURE 4: Three-dimensional representation of the HDX results. A pseudomonomer of *Mt*IPMS is rendered as a ribbon with the catalytic domain from chain A (green) and the linker and regulatory domain from chain B (yellow). Numbers on panel A correspond to the residue number, and black lines depict missing electron density. Regions rendered as surface correspond to peptides that display a decrease in deuterium incorporation (blue) or an increase in deuterium incorporation (red). One molecule of L-leucine is displayed in the regulatory domain. The substrate α-KIV, the Mg^{2+} ion, R80, D81, and Y410′ are also shown to denote the active site. The effects of L-leucine binding to the wild-type enzyme (panel A) and the Y410F enzyme (panel B) are shown. Panel C displays the effect of the Y410F substitution on the enzyme in the absence of L-leucine.

upon biophysical, kinetic, and structural studies, *Mt*IPMS is proposed to be allosterically regulated by L-leucine through a similar mechanism. In the current report, solution-phase HDX experiments have been employed to identify specific regions in the protein that are affected by L-leucine binding in order to better understand the mechanism of allosteric regulation (Figure 4A).

The region of the enzyme most affected by L-leucine binding is, not surprisingly, the regulatory domain. The majority of peptides that make up the binding pocket for L-leucine exhibit a decrease in deuterium exchange upon L-leucine binding, consistent with the location of the L-leucine binding pocket in three-dimensional structure (*20*). Importantly, the region of the loop that closes over the L-leucine binding pocket displays a decrease in deuterium incorporation upon L-leucine binding (Figure 2A). Residues 617−632 are of particular interest in that these residues make contacts with the amino group of L-leucine as well as the subdomain II region of the linker domain. Residues 488−495, located distal to the L-leucine binding pocket, also show decreased deuterium incorporation from solvent when L-leucine is bound and form another set of contacts between the regulatory and linker domains.

As stated above, the linker domain can be divided into two subdomains. Subdomain I (residues 369−424) is located adjacent to the catalytic domain while subdomain II (residues 434−490) is adjacent to the regulatory domain. In subdomain II, residues 453−457 are implicated in the HDX results as a region that undergoes a shift in conformational equilibria upon L-leucine binding. These residues interact directly with the regulatory domain, consistent with a network leading toward the catalytic domain. A closer look at the interface between this region and the regulatory domain demonstrates that while there are several charged residues at the interface, the majority of the residues are hydrophobic in nature. Subdomain I, however, reveals no regions that are perturbed upon L-leucine binding. One possible explanation for this result is that subdomain I is involved in other interactions that are not affected when L-leucine binds or that linker subdomain I acts in a manner similar to a node in a standing wave in the allosteric network. Due to missing electron density and asymmetry in the structure, the interface between the two subdomains of the linker region cannot be elucidated.[2]

In contrast to the regulatory domain, only a single peptide in the catalytic domain undergoes a shift in conformational equilibrium in response to L-leucine binding. This region, covering residues 78−87, makes up a wall of the active site (Figure 1B). Of the ten residues in this peptide, five are strictly conserved, a number made more significant by the fact that *Mt*IPMS only contains 35 strictly conserved residues out of 644 (*22*). Based on the three-dimensional structure, roles for two of the residues can be proposed. The residue R80 is predicted to be responsible for orienting the substrate α-KIV, while D81 is one of the ligands to the catalytically necessary divalent metal ion. Residue Q84 also merits attention based on the fact that, in one monomer of the crystal structure, this residue exhibits a change upon L-leucine binding, but in the adjacent monomer its position is unaffected. Thus, it is not currently clear if this is an allosterically relevant event. Overall, while one would have predicted that any type of allosteric mechanism must affect regions in the catalytic domain, the demonstration of the modulation by L-leucine binding of a single, conserved active site region in the entire TIM-barrel fold is dramatic.

This result allows for the proposal of a specific, physical mechanism of inhibition involving perturbation of the active site metal. Although other members of this Claisen condensing enzyme family do not require a divalent metal for activity, for *Mt*IPMS it is essential (*32*). The correct orientation of the active

site metal is critical to catalysis as it is proposed to bind α-KIV and to polarize the carbonyl for attack by the incoming AcCoA nucleophile. Based on steady-state parameters, the enzyme prefers Mg^{2+} as substitution with Mn^{2+} or Co^{2+} decreases the value of V/K_{KIV} by 5- and 10-fold, respectively. On the other hand, Zn^{2+} and Cd^{2+} act as inhibitors with micromolar affinities; both of these metals prefer geometries other than the octahedral environment of the *Mt*IPMS active site.

The hypothesis that perturbation of this region of the active site plays a role in the mechanism of allosteric regulation was tested by performing solution-phase HDX experiments with an enzyme variant that is insensitive to inhibition by L-leucine. Recently, we reported the results of a site-directed mutagenesis study of conserved residues in *Mt*IPMS located at the interface of the linker and catalytic domains. One of the mutant enzymes investigated, Y410F *Mt*IPMS, resulted in an enzyme that was insensitive to L-leucine binding. Residue Y410 is located on the N-terminal linker domain adjacent to the active site and some 40 Å from the L-leucine binding site (Figure 1B). Control experiments confirmed that Y410F *Mt*IPMS readily binds L-leucine (K_d = 20 μM), is chemically competent, and exists as a stable dimer, ruling out these alternate explanations for the absence of inhibition (*22*). This led to the hypothesis that the Y410F substitution had somehow disrupted the allosteric network such that L-leucine binding was uncoupled from inhibitory changes at the active site. The solution-phase HDX results also support this hypothesis (Figure 4B).

Under identical experimental conditions, binding of L-leucine to Y410F *Mt*IPMS results in nearly indistinguishable changes in the dynamics of the regulatory domain compared to the wild-type enzyme, consistent with the fact that the Y410F substitution has not drastically altered the affinity for L-leucine (Figure 4B). The Y410F enzyme also exhibits changes in the conformation of the C-terminal linker domain similar to those seen with the wild-type enzyme. However, in the catalytic domain residues 78−87 show no changes in conformational equilibrium in the Y410F enzyme. Instead, a region covering residues 236−258 is perturbed in the presence of L-leucine, and based on kinetic experiments, this perturbation does not alter the activity of the enzyme.

An analysis of the location of conformational perturbations induced by the mutation of the wild-type enzyme in the absence of L-leucine provides insight into the role of the Y410-containing loop in the linker domain and support for the proposed allosteric mechanism (Figure 4C). Consistent with the results above suggesting that the regulatory domains of the mutant and wild-type enzymes react similarly to L-leucine binding, the mutation does not influence the conformation of the regulatory domain relative to the wild-type enzyme. However, the Y410F substitution causes large regions of the linker domain to become more accessible to solvent. Most pertinent to the allosteric mechanism is the perturbation of subdomain II of the linker domain, a region proposed to be responsible for the transduction of the network out of the regulatory domain (see above). The importance of the conformational equilibrium of subdomain I of the linker domain in the allosteric mechanism is also supported by the near total perturbation of this region by the mutation.

Another key region affected by the Y410F substitution includes residues 78−87 in the catalytic domain. Relative to the wild-type enzyme, this region is more protected from solvent. This result suggests that the Y410F substitution mimics the effect of L-leucine binding on the active site. This proposal is supported by the fact that the k_{cat} value for the Y410F enzyme is similar to the rate of the wild-type enzyme in the presence of saturating concentrations of L-leucine (4.5 vs 15.2 min^{-1}, respectively) (*22*).

While *Mt*IPMS is the sole full-length structural report for this fold, the involvement of the Y410-containing loop and residues 78−87 in the allosteric mechanism of *Mt*IPMS is supported by studies of the bifunctional aldolase/dehydrogenase DmpG/DmpF from *Pseudomonas aeruginosa* (*33*). DmpG and *Mt*IPMS share the basic TIM-barrel structure catalytic domain and have nearly identical active site architecture resulting in DmpG as the top hit when *Mt*IPMS is used as a query with the secondary structure matching algorithm of the Protein Data Bank (*20*). In addition, DmpG has a linker domain with α-helical structure similar to that of *Mt*IPMS. DmpG/DmpF catalyzes the formation of acetaldehyde and pyruvate from 4-hydroxy-2-ketovalerate. The acetaldehyde produced in the DmpG active site is proposed to move through a 29 Å tunnel to the DmpF active site. Access to this tunnel is controlled through an allosteric mechanism initiated by the presence of NAD^+ at the DmpF active site coupled to the dynamic interactions of Y291 on the linker domain and H21 on the catalytic domain of DmpG. When the three-dimensional structures of DmpG and *Mt*IPMS are superimposed, Y291 (DmpG) is in a position similar to Y410 (*Mt*IPMS) and H21 (DmpG) is located at the C-terminus of a helix in the active site, similar to Q84 (*Mt*IPMS). Both Y291 and H21 are proposed to play specific acid/base roles in the catalytic mechanism of DmpG facilitating the movements needed in the allosteric mechanism. To date, Y410 and Q84 have no obvious role in the catalytic mechanism of *Mt*IPMS, but an involvement in the signal transduction network and allosteric mechanism is consistent with the results presented here.

The experimental identification of an allosteric signal spanning over 50 Å from the inhibitor binding site to the active site provides one of the first examples of a concrete and testable allosteric mechanism based on changes in protein dynamics and contact networks over a long range. Key to the validation of this pathway is the result from the L-leucine-insensitive mutant form of the enzyme which exhibits an altered pathway for the transduction of the inhibitory signal away from catalytically important residues in the active site. The continued development of high-resolution mass spectrometry and computer-aided data analysis makes this type of experiment more accessible and promises to provide additional detailed descriptions of this type of allosteric mechanism. As more examples are reported, it is possible that common characteristics of this type of regulation can be defined and exploited for allosterically targeted drug design. Additionally, these features could be incorporated into novel modular proteins, especially those with a TIM-barrel catalytic domain, with engineered allosteric regulation.

SUPPORTING INFORMATION AVAILABLE

Information regarding the peptide sequence coverage and deuterium uptake curves for each peptide described in the manuscript. This material is available free of charge via the Internet at http://pubs.acs.org.

REFERENCES

1. Monod, J., Changeux, J. P., and Jacob, F. (1963) Allosteric proteins and cellular control systems. *J. Mol. Biol. 6*, 306–329.
2. Kantrowitz, E. R., and Lipscomb, W. N. (1990) *Escherichia coli* aspartate transcarbamoylase: the molecular basis for a concerted allosteric transition. *Trends Biochem. Sci. 15*, 53–59.

3. Xu, Z., Horwich, A. L., and Sigler, P. B. (1997) The crystal structure of the asymmetric GroEL-GroES-(ADP)7 chaperonin complex. *Nature 388*, 741–750.
4. Popovych, N., Sun, S., Ebright, R. H., and Kalodimos, C. G. (2006) Dynamically driven protein allostery. *Nat. Struct. Mol. Biol. 13*, 831–838.
5. Tsai, C. J., del Sol, A., and Nussinov, R. (2008) Allostery: absence of a change in shape does not imply that allostery is not at play. *J. Mol. Biol. 378*, 1–11.
6. Fenton, A. W., Paricharttanakul, N. M., and Reinhart, G. D. (2004) Disentangling the web of allosteric communication in a homotetramer: heterotropic activation in phosphofructokinase from *Escherichia coli*. *Biochemistry 43*, 14104–14110.
7. Daily, M. D., Upadhyaya, T. J., and Gray, J. J. (2008) Contact rearrangements form coupled networks from local motions in allosteric proteins. *Proteins 71*, 455–466.
8. Ferguson, A. D., Amezcua, C. A., Halabi, N. M., Chelliah, Y., Rosen, M. K., Ranganathan, R., and Deisenhofer, J. (2007) Signal transduction pathway of TonB-dependent transporters. *Proc. Natl. Acad. Sci. U.S.A. 104*, 513–518.
9. Agarwal, P. K., Billeter, S. R., Rajagopalan, P. T., Benkovic, S. J., and Hammes-Schiffer, S. (2002) Network of coupled promoting motions in enzyme catalysis. *Proc. Natl. Acad. Sci. U.S.A. 99*, 2794–2799.
10. Goodey, N. M., and Benkovic, S. J. (2008) Allosteric regulation and catalysis emerge via a common route. *Nat. Chem. Biol. 4*, 474–482.
11. Bruschweiler, S., Schanda, P., Kloiber, K., Brutscher, B., Kontaxis, G., Konrat, R., and Tollinger, M. (2009) Direct observation of the dynamic process underlying allosteric signal transmission. *J. Am. Chem. Soc.* , (in press).
12. Lam, T. T., Lanman, J. K., Emmett, M. R., Hendrickson, C. L., Marshall, A. G., and Prevelige, P. E. (2002) Mapping of protein: protein contact surfaces by hydrogen/deuterium exchange, followed by on-line high-performance liquid chromatography-electrospray ionization Fourier-transform ion-cyclotron-resonance mass analysis. *J. Chromatogr. A 982*, 85–95.
13. Zhang, Z., Li, W., Logan, I. M., Li, M., and Marshall, A. G. (1997) Human recombinant [C22A] FK506-binding protein amide hydrogen exchange rates from mass spectrometry match and extend those from NMR. *Protein Sci. 6*, 2203–2217.
14. Lanman, J., Lam, T. T., Barnes, S., Sakalian, M., Emmett, M. R., Marshall, A. G., and Prevelige, P. E.Jr. (2003) Identification of novel interactions in HIV-1 capsid protein assembly by high-resolution mass spectrometry. *J. Mol. Biol. 325*, 759–772.
15. Lisal, J., Lam, T. T., Kainov, D. E., Emmett, M. R., Marshall, A. G., and Tuma, R. (2005) Functional visualization of viral molecular motor by hydrogen-deuterium exchange reveals transient states. *Nat. Struct. Mol. Biol. 12*, 460–466.
16. Gajiwala, K. S., Wu, J. C., Christensen, J., Deshmukh, G. D., Diehl, W., DiNitto, J. P., English, J. M., Greig, M. J., He, Y. A., Jacques, S. L., Lunney, E. A., McTigue, M., Molina, D., Quenzer, T., Wells, P. A., Yu, X., Zhang, Y., Zou, A., Emmett, M. R., Marshall, A. G., Zhang, H. M., and Demetri, G. D. (2009) KIT kinase mutants show unique mechanisms of drug resistance to imatinib and sunitinib in gastrointestinal stromal tumor patients. *Proc. Natl. Acad. Sci. U.S.A. 106*, 1542–1547.
17. Stieglitz, B. I., and Calvo, J. M. (1974) Distribution of the isopropylmalate pathway to leucine among diverse bacteria. *J. Bacteriol. 118*, 935–941.
18. McAdam, R. A., Weisbrod, T. R., Martin, J., Scuderi, J. D., Brown, A. M., Cirillo, J. D., Bloom, B. R., and Jacobs, W. R.Jr. (1995) In vivo growth characteristics of leucine and methionine auxotrophic mutants of *Mycobacterium bovis* BCG generated by transposon mutagenesis. *Infect. Immun. 63*, 1004–1012.
19. de Carvalho, L. P., Argyrou, A., and Blanchard, J. S. (2005) Slow-onset feedback inhibition: inhibition of *Mycobacterium tuberculosis* alpha-isopropylmalate synthase by L-leucine. *J. Am. Chem. Soc. 127*, 10004–10005.
20. Koon, N., Squire, C. J., and Baker, E. N. (2004) Crystal structure of LeuA from *Mycobacterium tuberculosis*, a key enzyme in leucine biosynthesis. *Proc. Natl. Acad. Sci. U.S.A. 101*, 8295–8300.
21. de Carvalho, L. P., and Blanchard, J. S. (2006) Kinetic and chemical mechanism of alpha-isopropylmalate synthase from *Mycobacterium tuberculosis*. *Biochemistry 45*, 8988–8999.
22. de Carvalho, L. P., Frantom, P. A., Argyrou, A., and Blanchard, J. S. (2009) Kinetic evidence for interdomain communication in the allosteric regulation of alpha-isopropylmalate synthase from *Mycobacterium tuberculosis*. *Biochemistry 48*, 1996–2004.
23. Lee, G. M., and Craik, C. S. (2009) Trapping moving targets with small molecules. *Science 324*, 213–215.
24. Zhang, H. M., Kazazic, S., Schaub, T. M., Tipton, J. D., Emmett, M. R., and Marshall, A. G. (2008) Enhanced digestion efficiency, peptide ionization efficiency, and sequence resolution for protein hydrogen/deuterium exchange monitored by Fourier transform ion cyclotron resonance mass spectrometry. *Anal. Chem. 80*, 9034–9041.
25. Zhang, H. M., Bou-Assaf, G. M., Emmett, M. R., and Marshall, A. G. (2009) Fast reversed-phase liquid chromatography to reduce back exchange and increase throughput in H/D exchange monitored by FT-ICR mass spectrometry. *J. Am. Soc. Mass Spectrom. 20*, 520–524.
26. Emmett, M. R., and Caprioli, R. M. (1994) Micro-electrospray mass spectrometry: Ultra-high-sensitivity analysis of peptides and proteins. *J. Am. Soc. Mass Spectrom. 5*, 605–613.
27. Schaub, T. M., Hendrickson, C. L., Horning, S., Quinn, J. P., Senko, M. W., and Marshall, A. G. (2008) High-performance mass spectrometry: Fourier transform ion cyclotron resonance at 14.5 T. *Anal. Chem. 80*, 3985–3990.
28. Senko, M. W., Hendrickson, C. L., Emmett, M. R., Shi, S. D. H., and Marshall, A. G. (1997) External accumulation of ions for enhanced electrospray ionization Fourier transform ion cyclotron resonance mass spectrometry. *J. Am. Soc. Mass Spectrom. 8*, 970–976.
29. Beu, S. C., and Laude, D. A.Jr. (1992) Elimination of axial ejection during excitation with a capacitively coupled open trapped-ion cell for Fourier transform ion cyclotron resonance mass spectrometry. *Anal. Chem. 64*, 177–180.
30. Schwartz, J. C., Senko, M. W., and Syka, J. E. P. (2002) A two-dimensional quadrupole ion trap mass spectrometer. *J. Am. Soc. Mass Spectrom. 13*, 659–669.
31. Marshall, A. G., and Guan, S. (1996) Advantages of high magnetic field for Fourier transform ion cyclotron resosnace mass spectrometry. *Rapid Commun. Mass Spectrom. 10*, 1819–1823.
32. de Carvalho, L. P., and Blanchard, J. S. (2006) Kinetic analysis of the effects of monovalent cations and divalent metals on the activity of *Mycobacterium tuberculosis* alpha-isopropylmalate synthase. *Arch. Biochem. Biophys. 451*, 141–148.
33. Manjasetty, B. A., Powlowski, J., and Vrielink, A. (2003) Crystal structure of a bifunctional aldolase-dehydrogenase: sequestering a reactive and volatile intermediate. *Proc. Natl. Acad. Sci. U.S.A. 100*, 6992–6997.